International Journal of Solids and Structures 46 (2009) 3357–3364

Contents lists available at ScienceDirect

International Journal of Solids and Structures

journal homepage: www.elsevier.com/locate/ijsolstr

Modeling of high-density compaction of granular materials by the Discrete Element Method

B. Harthong *, J.-F. Jérier, P. Dorémus *, D. Imbault, F.-V. Donzé

Laboratoire 3S-R, Domaine universitaire, BP 53, 38041 Saint Martin d'Heres cedex 9, France

ARTICLE INFO

Article history:
Received 8 January 2009
Received in revised form 27 March 2009
Available online 18 May 2009

Keywords:
Discrete Element Method
Force–displacement relationship
High-density compaction
Granular media

ABSTRACT

Cold compaction of metal powders is now commonly studied at a microscopic scale, to further our understanding of contact mechanics between grains. The Discrete Element Method (DEM) is therefore, a good compromise between calculation time and precision. DEM simulations are in general limited to a relative density of about 0.8, because the existing contact laws do not reproduce all the physical phenomena involved in the densification of granular media. Local contact mechanics can be studied by finite element analyses on meshed distinct elements (MDEM, Meshed Distinct Element Method). However, this method is too time-consuming when in the presence of a large number of grains. In the following work, a new analytical contact law will be formulated with MDEM which will subsequently be used to validate the DEM model. Thus, it will be possible with DEM modeling to reproduce high-density compaction of random packings up to a relative density of about 0.95. By introducing a local relative density parameter in the force–displacement relationship, the incompressibility effects which rule high-density behaviors can be introduced in the modeling of powder compaction.

1. Introduction

Granular media, and in particular industrial powders, are often modeled using two different approaches. The first one is based on macroscopic and continuum models, generally derived from soil mechanics, as for example the Drucker–Prager Cap model (Drucker and Prager, 1952). In order to complete and improve the macroscopic models, a second approach has been developed to account for the bulk properties of powders by modeling the interaction phenomena between grains. Two methods exist in this type of microscopic approach: the Discrete Element Method (Cundall and Strack, 1979; Donzé et al., 2009) and another method based on continuum mechanics and finite element simulation of the compaction of meshed discrete particles (Gethin et al., 2003; Procopio and Zavaliangos, 2005). In the following, this latter method will be called MDEM (Meshed Distinct Element Method).

The DEM was first introduced for the modeling of granular materials (Cundall and Strack, 1979), and is quite successful because of its ability to reproduce particles rearrangement (Wu et al., 2003; Martin, 2004; Belheine et al., 2009). This method requires a local model of the contact behavior between two particles. In this contact model, the relation between the normal contact force and the relative displacement is of great importance. For non-linear elastic problems, Hertz' formula (Landau and Lifchitz, 1967) can be used. Other contact laws have been formulated specifically for the DEM, in order to adapt it accurately to elastic–plastic problems (for instance Vu-Quoc et al. (2001) for small plastic deformations).

For a plastic Von Mises-type material with strain hardening, some authors (Storåkers et al., 1997) suggest using a purely plastic law, without considering any elasticity: $\sigma = K\varepsilon^n$, where σ and ε are, respectively, the uniaxial stress and strain, K and n the material hardening parameters. Thus Storåkers et al. (1997) proposed a contact model which has been used by several authors to model the compaction of granular media (Storåkers et al., 1999; Heyliger and McMeeking, 2001; Martin, 2004; Martin and Bouvard, 2003; Martin et al., 2003; Skrinjar and Larsson, 2004). Nevertheless, those approaches are limited in relative density, because this type of model is based on the assumption that the contacts between the particles can be considered as independent. In other words, each contact reacts as if it was isolated, the contact zones being far enough from each other that they do not interact. For a relative density higher than about 0.8, the mutual influence of the contacts cannot be neglected (Mesarovic and Fleck, 2000; Martin et al., 2003). Moreover, Storåkers' model has been formulated for small strain kinematics (Storåkers et al., 1997), and this assumption may be considered as critical for high densities.

Finite element simulations at the particle scale were performed by Mesarovic and Fleck (1999, 2000). Mesarovic and Fleck (2000) also carried out a finite element study of a periodic structure. The first MDEM studies on granular random packings were done in 2D (Gethin et al., 2003; Procopio and Zavaliangos, 2005). Then

* Corresponding authors.
E-mail addresses: harthong@geo.hmg.inpg.fr (B. Harthong), pierre.doremus@hmg.inpg.fr (P. Dorémus).

0020-7683/$ - see front matter © 2009 Elsevier Ltd. All rights reserved.
doi:10.1016/j.ijsolstr.2009.05.008

the problem of 3D packings has been analyzed in particular by Chen et al. (2006); Frenning (2008) and Chen (2008). The MDEM gives an accurate description of the particles' deformation and produce accurate results up to high densities. Unfortunately, because of its high computational cost, this type of simulation is limited to assemblies of about a hundred particles.

Even though the MDEM allows a more complete and more accurate study, the DEM remains an interesting approach because of its ability to perform simulations on a more realistic number of particles, closer to a representative elementary volume. However, the MDEM will still be used to derive a new force–displacement contact law for the DEM. Since the study of the mutual influence of the contacts in random packings would require numerous simulations and a lot of computational time, the new force–displacement model is derived using periodic lattices and only under certain loading conditions. Then, this model is extrapolated to random packings, under every loading.

Thus, this approach consists in analyzing the densification of a simple cubic lattice by using MDEM simulations. The results obtained with this simple and cheap (in terms of CPU time) lattice lets the user choose which will be the best local constitutive law to be used in the DEM. The robustness of this law is checked by comparisons with more complex packings. Some validation simulations will be performed first on body-centered cubic lattices, and then on random packings. Fig. 1 summarizes this approach.

2. Material

An elastic–plastic Von Mises-type constitutive law with strain hardening is used to represent the spheres' material. The relationship between stress and strain in the uniaxial case is given by:

$$\sigma = \sigma_Y + K_1 \varepsilon_{pl}^{n_1}, \tag{1}$$

where σ is the uniaxial stress, σ_Y the yield stress, ε_{pl} the equivalent plastic strain, and K_1 and n_1 are the hardening parameters.

For the validation of the proposed approach, stress–strain law (2) will be used for the formulation of the DEM contact law, as in Storåkers et al. (1997). With this constitutive model, a simpler modeling of plasticity effects can be done:

$$\sigma = K_2 \varepsilon^{n_2}, \tag{2}$$

σ and ε being the uniaxial stress and strain, K_2 and n_2 the hardening parameters.

In the following, the material behavior will be entirely determined by constants K_2 and n_2. The DEM approach is based on Eq. (2) whereas Eq. (1) is used in the MDEM simulations. Then Eqs. (1) and (2) are set equal to one another. By adjusting the values of the coefficients in Eqs. (1) and (2), a similar loading curve should be obtained. The numerical values of K_2 and n_2 which will be used are those corresponding to lead ($K_2 = 20.5$ MPa, $n_2 = 0.24$). This corresponds to $\sigma_Y = 5$ MPa, $K_1 = 15.5$ MPa and $n_1 = 0.35$. The elastic behavior in the MDEM is supposed to be linear and isotropic with Young's modulus $E = 10,000$ MPa and Poisson's coefficient $\nu = 0.435$. By choosing this material, an experimental validation can be easily planned.

In the numerical model, the powder particles are represented by spheres of identical radius R = 5 mm (except when mentioned), without friction.

3. Simple, die and hydrostatic compaction of a simple cubic structure

Without friction, the simple cubic lattice can be reduced to an elementary cell composed of a sphere compressed by rigid planes. Adding symmetry conditions, the MDEM model can be reduced to an eighth of a sphere (Fig. 2a). The MDEM simulations are performed with the finite element code ABAQUS.

The finite element meshes used for this study are shown in Fig. 2b. The finer mesh of one eighth of a sphere is made up of 1200 tetrahedral quadratic elements and has been used to study simple periodic structures for curve-fitting applications. The mesh of a whole sphere is a little coarser (2600 quadratic elements for the whole sphere) and has been used to perform simulations involving several particles. In both cases, the meshes have been designed to investigate large displacements and to reduce computation time. The mesh is refined on the surface to represent correctly the evolution of the contact surfaces in every direction.

3.1. MDEM results

Force–displacement curves can be seen on Fig. 3 for a die compaction, hydrostatic compaction and simple compression (compression of an isolated sphere).

The simple compression represents the behavior obtained for isolated contacts, and thus corresponds to Storåkers' assumptions (Storåkers et al., 1997). In the early stage of compaction, the three curves are superimposed (h/R less than about 0.15). This zone corresponds to the validity domain when independent contacts are assumed. For higher values of h/R (h/R greater than about 0.15 for hydrostatic compaction and about 0.35 for die compaction) the interaction between the different contacts becomes significant and the curves diverge from the simple compression curve. This phenomenon is analyzed in Mesarovic and Fleck (2000). Then, at the end of compaction, it can be observed that the force increases to infinity for hydrostatic and die compaction.

3.2. Formulation of a DEM contact law

Fig. 3 clearly shows that the force developed at the contact between two spheres for different loading types cannot depend only on the relative displacement h, except at the beginning of compaction when the contacts are independent.

The configuration of the deformed spheres (Fig. 3) suggests that the increase of the force at the end of compaction is related to plas-

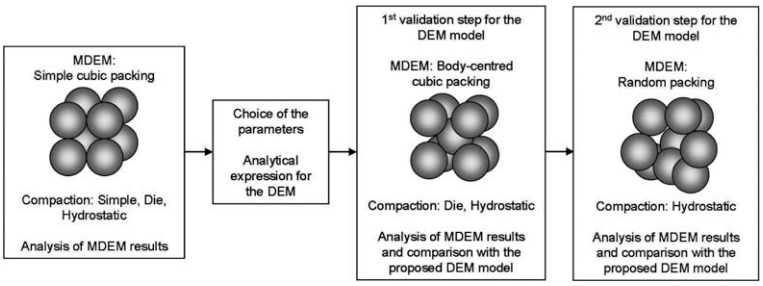

Fig. 1. Methodology.

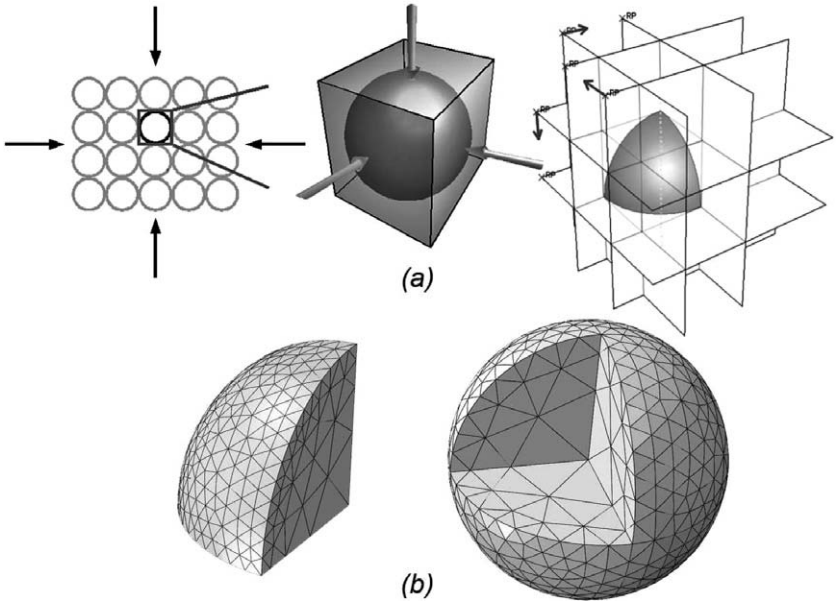

Fig. 2. (a) Geometric simplifications for MDEM modeling (example of hydrostatic compaction). (b) Finite element meshes.

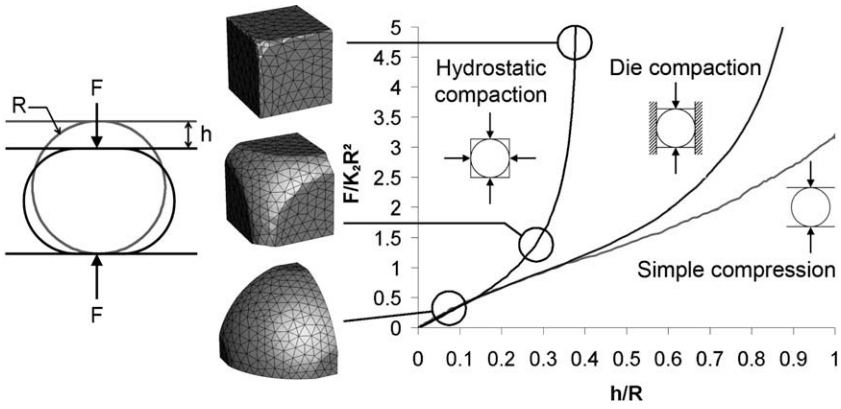

Fig. 3. Comparison of the force–displacement behavior of a sphere–sphere contact for three loading types on an SC cell (die compaction, hydrostatic compaction and simple compression).

tic incompressibility of the material when free space is no longer available and relative displacement cannot take place anymore. The relative density can account for this phenomenon for die or hydrostatic compaction, with a relation which verifies the following property:

$F \to \infty$ when $\rho \to 1$, where ρ is the relative density.

This relative density can be calculated as the ratio between the volume of the sphere (assumed to be constant) and the volume of the polyhedral cell formed by the rigid compressing planes. With the loadings and the lattice considered here, this ratio is given by the following relations:

$$\rho = \frac{4/3\pi R^3}{(2R-h)^3} \text{ in the hydrostatic case;} \quad (3)$$

$$\rho = \frac{4/3\pi R^3}{(2R-h)(2R)^2} \quad \text{for die compaction.} \quad (4)$$

To calculate ρ in the DEM framework, it is possible to use the concept of Voronoï cell (Gellatly and Finney, 1982b,a). If, for each contact, a contact plane is defined, as represented in the MDEM models by rigid planes, each sphere is then isolated in a polyhedron the volume of which can be calculated (Fig. 4a). The ratio of the sphere's volume (constant) and the Voronoï cell's volume (variable) gives the relative density ρ for each sphere in a random packing.

When considering an interaction between two spheres, the contact force tends to infinity when the density of both particles reaches one. Then, the arithmetic average relative density can be defined as:

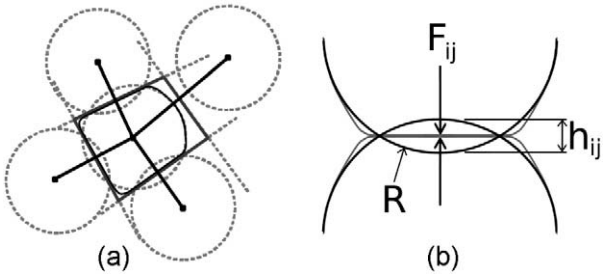

Fig. 4. (a) 2D illustration of a Vorono cell. (b) Notations for the DEM model.

$\rho_{ij} = \frac{1}{2}(\rho_i + \rho_j)$ for two particles of relative density ρ_i and ρ_j. (5)

Thus the behavior of the contact is studied in two limit cases: In the first part of compaction, the contacts are independent and the contact force depends only on h; then at the end, when ρ tends to 1, plastic incompressibility prevails and the contact force essentially depends on ρ.

The intermediate situation, which corresponds to the evolution of the interaction between the different contacts, is considered to depend on both parameters h/R and ρ. It is modeled here in a simple way as an interpolation between the two limiting cases mentioned above.

The notations used for the DEM model are shown in Fig. 4b. The overlap h_{ij} is the equivalent of the indentation depth h used for MDEM simulations and illustrated in Fig. 3. The force can then be expressed with an incremental formulation:

If $h_{ij} \geqslant 0$:

$$F_{ij}(t+\Delta t) = F_{ij}(t) + S_{ij}(h_{ij}, \rho_{ij}).\Delta h_{ij}(t+\Delta t) \tag{6}$$

If $h_{ij} < 0$:

$$F_{ij}(h_{ij}, \rho_{ij}) = 0 \tag{7}$$

where the stiffness S_{ij} is assumed to be a sum of two independent terms:

$$S_{ij} = S_1(h_{ij}) + S_2(\rho_{ij}) \tag{8}$$

S_1 represents the stiffness balancing the deformation of two isolated spheres in contact (simple compression curve in Fig. 3). S_2 is the stiffness developed by plastic incompressibility, which tends to infinity when ρ_{ij} tends to one. It is assumed here that the impingement of the different contacts can be modeled as an increasing resistance to the deformation depending on the relative density ρ_{ij} defined for each pair of spheres in contact. Each single contact involving a sphere i modifies its relative density ρ_i, and this modification affects all the contacts of the sphere i.

(7) expresses the classical DEM contact criterion: if $h_{ij} < 0$, the distance between two particle centers is greater than the sum of the (initial) radii, and then it is considered that there is no contact.

Moreover, it is assumed that the scaled form:

$$\frac{F}{K_2 R^2}\left(\frac{h_{ij}}{R}, \rho_{ij}\right) \tag{9}$$

is independent of both parameters K_2 and R. This assumption is confirmed by MDEM results as shown in Fig. 5 and has the following physical meaning:

- The same distribution of stress is obtained on the contact surface for the same value of the relative indentation depth h_{ij}/R;
- The force F is proportional to the contact surface, and the contact surface is proportional to R^2 (and consequently F is proportional to R^2);
- The stress is proportional to the material parameter K_2, because of the material behavior defined by Eq. (2), and consequently the average contact stress F/R^2 is proportional to K_2.

Then, based on curve-fitting of the MDEM results, the following law is formulated:

$$S_{ij} = K_2 R\left[\alpha_1(n_2)e^{\beta_1(n_2)\frac{h_{ij}}{R}} + \gamma_1(n_2)e^{-\delta_1\frac{h_{ij}}{R}} + \alpha_2(n_2)\frac{[max(0, \rho_{ij} - \rho_{0_{ij}})]^2}{1-\rho_{ij}}\right] \tag{10}$$

where $\alpha_1, \beta_1, \gamma_1, \delta_1, \alpha_2$ are constants or functions of n_2. $\rho_{0_{ij}}$ is the average relative density when the contact is identified.

In the following, the coefficients used will be:

$$\begin{cases} \alpha_1(n_2) = 0.97 - 0.58n_2 \\ \beta_1(n_2) = 1.75\left(1 + \frac{n_2}{2}\right) \\ \gamma_1(n_2) = \frac{15}{1+3n_2} - 4 \\ \delta_1 = 8 \\ \alpha_2(n_2) = 15\left(1 - \frac{n_2}{2}\right) \end{cases} \tag{11}$$

The evolution of the force calculated with Eq. (10) with the hardening parameter n_2 is shown in Fig. 6 in comparison with MDEM results for $n_2 = 0, 0.1, 0.24, 0.5$ and 0.8.

The S_1 part of the stiffness S_{ij} is:

$$S_1 = K_2 R\left[\alpha_1(n_2)e^{\beta_1(n_2)\frac{h_{ij}}{R}} + \gamma_1(n_2)e^{-\delta_1\frac{h_{ij}}{R}}\right] \tag{12}$$

which is a sum of two terms reflecting the behavior of a sphere in simple compression, according to the MDEM results presented in Fig. 6a. It can be seen in Fig. 6a that in the case of the simple compression, the stiffness decreases at the beginning of compaction and then increases. The initial decrease of the stiffness is much more significant for small values of n_2 and tends to vanish when n_2 approaches 1. In any case, the proposed form of Eq. (10) is just the result of the fitting procedure. Here the choice has been made to take

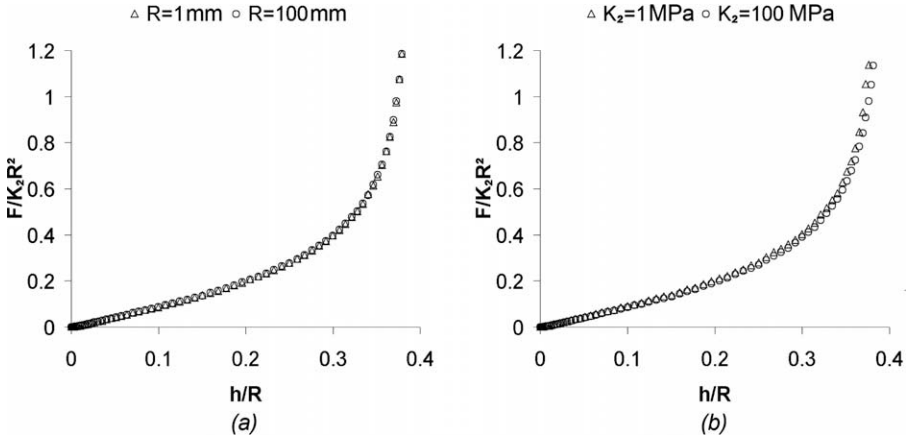

Fig. 5. Illustration of the influence of parameters R and K_2. (a) Influence of R for $K_2 = 20.5$ MPa. (b) Influence of K_2 for $R = 5$ mm. The small difference in the two curves is easily explained by elastic compressibility because the same elastic parameters E and ν have been used for both cases, and thus the yield stress σ_Y in Eq. (1) and the yield strain are higher for $K_2 = 100$ MPa. This effect of elastic compressibility is neglected in the present work.

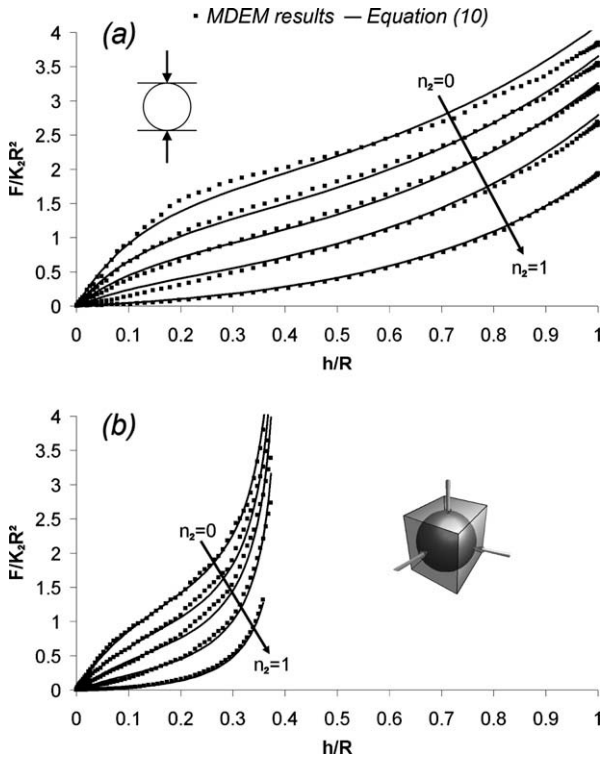

Fig. 6. Evolution of MDEM results and analytical results based on Eq. (10) in the case of (a) simple compression and (b) hydrostatic compaction of a simple cubic cell for $n_2 = 0, 0.1, 0.24, 0.5, 1$.

into account extreme values of n_2 and a range of h/R from 0 to 1. In particular, the form of the S_2 term could be much more simplified by restraining the values of n_2 or h/R.

The S_2 term is:

$$S_2 = K_2 R\left[\alpha_2(n_2)\frac{(max(0,\rho_{ij}-\rho_{0_{ij}}))^2}{1-\rho_{ij}}\right] \tag{13}$$

which is zero for $\rho_{ij} < \rho_{0_{ij}}$ and tends to infinity when ρ_{ij} tends to 1 to verify the incompressibility condition. For small values of $\rho_{ij} - \rho_{0_{ij}}$, S_2 remains small to ensure that it remains negligible compared to S_1 in the first stage of compaction.

Fig. 7 shows the force–displacement curves obtained with (10) and with MDEM simulations for simple compression, hydrostatic and die compaction of a simple cubic lattice in the example of lead. For comparison, Storåkers' model results are also presented (Eq. (14)). This model gives the same results in every case as it only depends on h:

$$F_{ij} = 2^{1-3\frac{n_2}{2}}3^{1-n_2}\pi c^{2+n_2}K_2 R_0^{1-\frac{n_2}{2}}h_{ij}^{1+\frac{n_2}{2}} \tag{14}$$

where $\frac{1}{R_0} = \frac{1}{R_i} + \frac{1}{R_j}$ and $c^2 = 1.43e^{-0.97n_2}$.

Fig. 7 illustrates the ability of Eq. (10) to model loading types which are quite different. It is considered that the relative density is zero for simple compression (the volume of the Voronoï cell is infinity). According to the MDEM results, Eq. (14) is overestimating the simple compression curve (which it should match) for large displacements. This is a consequence of the assumption of small strain kinematics initially used by Storåkers et al. (1997). The differences between Storåkers' model and finite element results in the case of deformable spheres is discussed in details in Mesarovic and Fleck (2000).

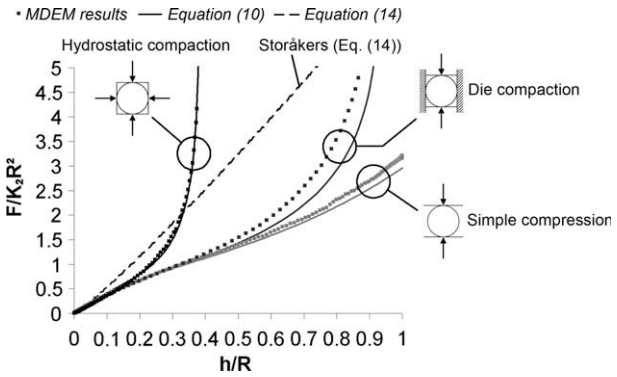

Fig. 7. Comparison between MDEM results for an SC cell, Eqs. (10) and (14). Eq. (10) shows good agreement with MDEM curves in the three cases, whereas Eq. (14) (Storåkers' model) gives the same result for all loading types.

4. Validation of the DEM model: hydrostatic and die compaction of a body-centered cubic lattice

First, the validation is focused on the force developed by a single contact in a body-centered cubic (BCC) lattice. To obtain this force, an MDEM simulation is analyzed, where a sphere is compressed by 14 rigid planes which represent the contacts with the neighboring spheres, as in a BCC lattice geometry (Fig. 8). A hydrostatic compaction has been chosen to simplify the simulation by avoiding rotations of the rigid planes which would be necessary to represent the sliding of the diagonal contacts.

Fig. 8 shows a comparison between MDEM curves and the analytical model based on Eq. (10). The results observed here are encouraging, and show that the formulation of a contact law based on a simple cubic lattice can fit other packings with some success.

However, it should be observed that the DEM model predicts that the force is zero for the second contact. This can be explained by the contact criterion (7) which neglects the sphere's deformation. The spheres' deformation creates a material flow in the directions which remain free, and a contact can be created between two particles even though criterion (7) is not respected (the distance between the centers is more than the sum of the radii). This phenomenon is illustrated in Fig. 9. In the case presented in Fig. 8, criterion (7) predicts that the second contacts appear for a relative density greater than one.

Thus the secondary contacts are quite badly reproduced by the DEM model. However, it is possible to assume that the sum of the forces developed by the secondary contacts is, at the macroscopic scale, a relatively small force, compared to the force developed by the initial contacts.

To estimate the importance of a good prediction of the secondary contacts, a macroscopic MDEM model is studied, which focuses on the global resulting contact force. This is made possible by periodic lattices, because they can be reduced to a complete elementary cell, and the resulting forces on the walls of this cell can be retrieved.

Because of the simplicity of the BCC lattice, the resulting forces can be derived analytically from Eq. (10), through simple geometric considerations. Fig. 10 compares the results of this analytic calculation with an equivalent MDEM simulation.

When new contacts occur, the MDEM global force curves exhibit a change of curvature (shown in Fig. 10 by the arrows). As the difference between the global force calculated with the MDEM and the one calculated analytically using (10) is quite small, the contact criterion (7) is assumed to be correct for most cases, because:

- either the new contact is created early in the compaction, then criterion (7) is accurate enough (for instance, the case of secondary contacts in a die compaction of a BCC lattice, Fig. 10b)

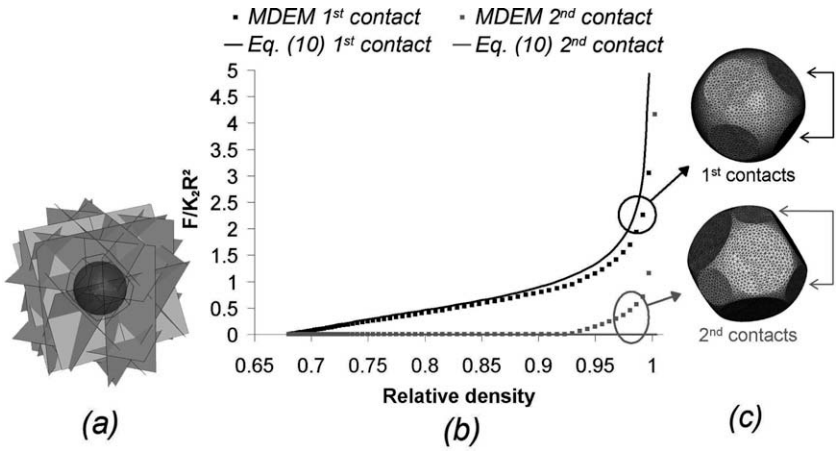

Fig. 8. Local contact force for a BCC cell under hydrostatic compaction. Comparison between MDEM local simulation and analytical model (10) of a BCC cell under hydrostatic compaction. (a) MDEM model, (b) results, (c) contacts appearance.

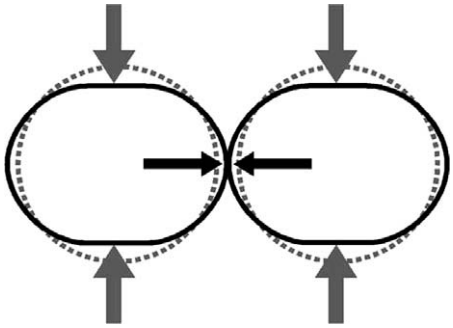

Fig. 9. Advance of the contact because of particles' deformation.

- or it is created later in the compaction, and then its influence on the global force remains quite small compared to the forces developed by the earlier contacts.

In order to strengthen this assumption, a random packing will now be studied.

5. Random packing under hydrostatic compaction

To represent the compaction of a random packing, a sphere is compressed by rigid planes randomly placed around it. To simplify the post-processing analysis, the rigid planes are translating without any rotation. The amplitude of the displacement is proportional to the initial distance between the planes and the center of the sphere. This assumes that the 'center' of the deformed sphere, with which the relative displacement h must be defined, remains at the same place. A 'center' is defined by the equilibrium of the forces. This compaction is close to a hydrostatic compaction of a random packing, without any rearrangement.

Moreover, it is considered here that the relative density used in Eq. (10) is equal to the relative density of the considered sphere. This assumption implies that there is only a small difference in relative density between two neighboring spheres. In the case of a monodisperse packing, this consideration appears to be reasonable.

The MDEM model has 14 contacts, featuring 12 initial contacts and 2 secondary contacts, which appear during compaction. For all

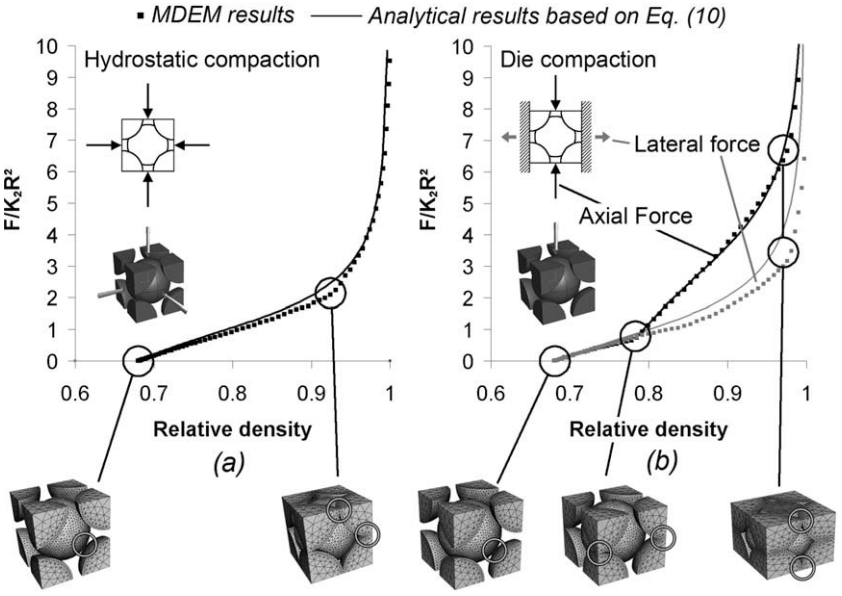

Fig. 10. Global force on a BCC cell. (a) Hydrostatic compaction. (b) Die compaction (axial force on the punches and lateral force on the lateral walls). When new contacts occur, the curves exhibit a change of curvature (indicated by the arrows). The corresponding contacts are indicated on the figures of the model's deformed geometry.

12 initial contacts, the evolution of h and ρ is identical. Thus according to Eq. (10), the force created by each of these contacts is the same. Fig. 11a shows the evolution of the forces of the initial contacts according to the MDEM as a function of the relative density, as compared to the force obtained with Equation (10). It can be observed that on one hand, the dispersion of the MDEM forces is quite low, and on the other hand, the evolution of the force predicted by Eq. (10) is close to the MDEM forces. Fig. 11b represents the evolution of the forces of both secondary contacts which appear during compaction. Because of the phenomenon mentioned in Section 4 and illustrated in Fig. 9, criterion (7) generates an important delay in the contact identification. The new contacts appear at a relative density of 0.87 and 0.91 instead of 0.8 and 0.83 for the MDEM.

As in the case of the BCC lattice analyzed in Section 4, the initial contacts are well predicted by the analytical model based on Eq. (10), whereas secondary contacts show some differences with the MDEM reference. As in Section 4 for the BCC lattice, global forces applied by the compressing walls will be studied on a random packing sample.

To keep a reasonable MDEM calculation time, the sample is limited to 15 identical spheres, with a radius $R = 0.19$ mm. For the DEM simulations, the geometrical complexity of a random packing requires using a discrete element code: thus these simulations were performed with the DEM code YADE (Kozicki and Donzé, 2008). This open-source code allowed the implementation of both the calculation of the local relative density and the contact law derived from Eq. (10). For comparison needs, Storåkers' model was also implemented.

The results of the simulation presented in Fig. 12 correspond to the hydrostatic compaction of the 15 sphere random packing, without friction. The curves show a good agreement between MDEM, DEM with Eq. (10) and DEM with Storåkers' law when the relative density is less than 0.85. After that, Storåkers' law diverges from the other models.

In this 15-sphere packing, when the relative density is 0.85, the maximum value of the overlap between two spheres is $h_{max}/R = 0.44$ for Eq. (14) and $h_{max}/R = 0.4$ for Equation (10). The average overlap is $h_{av}/R = 0.24$ for Equation (14) and $h_{av}/R = 0.22$ for Eq. (10). For these values of h/R, Eq. (14) overestimates the simple compression condition, as shown in Fig. 7, but because of plastic incompressibility and contact impingement, the real force is also greater than the simple compression force, such that, the difference between both remains small up to a relative density of 0.85. In a similar way, Fig. 7 shows that Eq. (14) fits the simple compression curve up to an h/R of about 0.15, and the hydrostatic compaction of the simple cubic structure up to $h/R = 0.35$. The same phenomenon explains the results presented in Fig. 12.

These results show that in a purely random case, with a realistic distribution of the initial and secondary contacts, Equation (10) together with the classical contact criterion (7) can bring accurate results about the global forces on the walls. Thus the assumption proposed at the end of Section 3 seems relevant.

6. Conclusion

The study of the contact forces in a random packing of spheres subjected to compaction is essential for numerical simulation. The MDEM is based on precise and quantifiable data. But for the moment, it still requires a really long calculation time compared to the DEM.

In the present work, an analytical expression for the contact forces could be extracted from the MDEM, and re-used in the DEM. The approach carried out here, based on periodic lattices, enables a better analysis of the different parameters governing the contact forces, with a reduced calculation time. The introduction of a new parameter which represents the local relative density can model the effects of plastic incompressibility in the DEM framework, thus allowing the description of high-density effects. This parameter has been calculated using the concept of Voronoï cell (Gellatly and Finney, 1982b,a). Despite some discrepancy in the predictions, related to the secondary contacts identification criterion, the results presented above are encouraging, and show that the approach proposed here can potentially lead to an interesting accuracy.

The basic assumptions, in particular the choice of a simplified material, without elasticity, have of course a real influence on the proposed contact law (Eq. (10)). However, they do not have a major influence on the chosen approach, in which a useful law for ran-

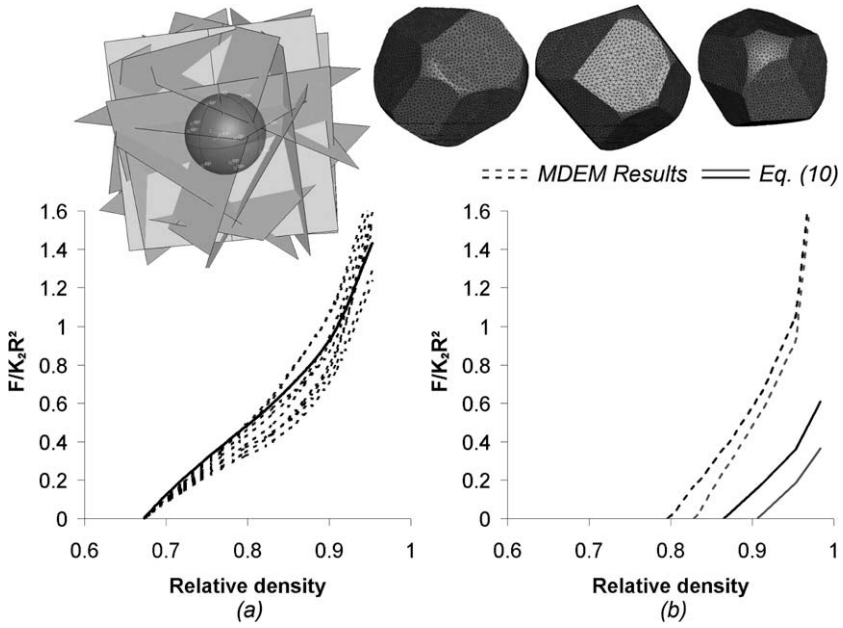

Fig. 11. Approach of a random packing: (a) initial contacts, (b) secondary contacts.

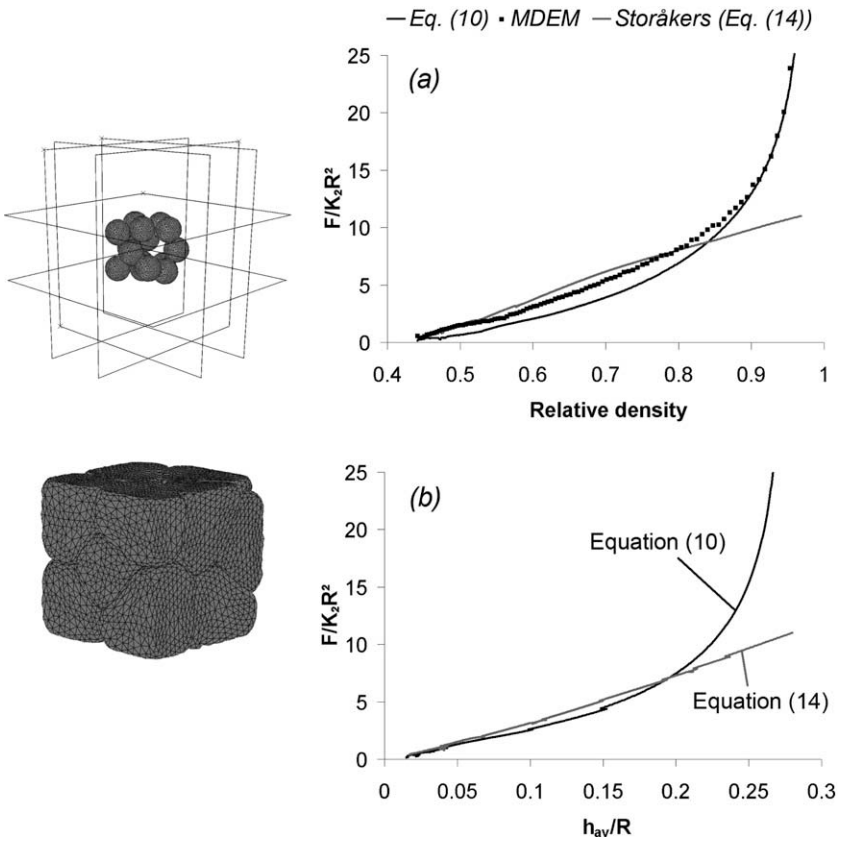

Fig. 12. MDEM results, computed with ABAQUS, and DEM results, computed with YADE, for hydrostatic compaction of 15 spheres in random packing, without friction. DEM curves are based on Eqs. (14) and (10). (a) MDEM and DEM forces as a function of the relative density. (b) DEM forces as a function of the average overlap in the packing.

dom packings is extracted from a simple periodic lattice. To perform realistic DEM simulations, this approach will be kept and the model will also need to account for the elasticity of the sphere's constitutive material, polydisperse sphere packings, different material types, and for the tangential and cohesive behavior of the contacts. These two latter parameters will then be adjusted to fit the behavior of a real powder which is composed of irregular grains and lubricants.

References

Belheine, N., Plassiard, J.P., Donzé, F.V., Darve, F., Seridi, A., 2009. Numerical simulation of drained triaxial test using 3d discrete element modeling. Computers and Geotechnics 36 (1–2), 320–331.

Chen, Y., 2008. Contribution a la modélisation de la compression des poudres par une methode d'éléments discrets maillés. Ph.D. thesis, Institut Polytechnique de Grenoble.

Chen, Y., Imbault, D., Dorémus, P., 2006. Numerical simulation of cold compaction of 3d granular packings. Materials Science Forum, 301–304.

Cundall, P.A., Strack, O.D.L., 1979. A discrete numerical model for granular assemblies. Geotechnique 29, 47–65.

Donzé, F.V., Richefeu, V., Magnier, S.-A., 2009. Advances in discrete element method applied to soil, rock and concrete mechanics, in: state of the art of geotechnical engineering. Electronic Journal of Geotechnical Engineering, 44.

Drucker, D.C., Prager, W., 1952. Soil mechanics and plastic analysis or limit design. Quarterly Journal of Mechanics and Applied Mathematics 10, 157–175.

Frenning, G., 2008. An efficient finite/discrete element procedure for simulating compression of 3d particle assemblies. Computer Methods in Applied Mechanics and Engineering 197, 4266–4272.

Gellatly, B.J., Finney, J.L., 1982a. Calculation of protein volumes: an alternative to the vorono procedure. Journal of Molecular Biology 161, 305–322.

Gellatly, B.J., Finney, J.L., 1982b. Characterisation of models of multicomponent amorphous metals: the radical alternative to the vorono polyhedron. Journal of Non-Crystalline Solids 50, 313–329.

Gethin, D.T., Lewis, R.W., Ransing, R.S., 2003. A discrete deformable element approach for the compaction of powder systems. Modelling and Simulation in Materials Science and Engineering 11, 101–114.

Heyliger, P.R., McMeeking, R.M., 2001. Cold plastic compaction of powders by a network model. Journal of the Mechanics and Physics of Solids 49, 2031–2054.

Kozicki, J., Donzé, F.-V., 2008. A new open-source software developed for numerical simulations using discrete modelling methods. Computer Methods in Applied Mechanics and Engineering 197, 4429–4443.

Landau, L., Lifchitz, E., 1967. Théorie de l'élasticité (Theory of Elasticity), second ed. Les Éditions Mir Moscou.

Martin, C.L., 2004. Elasticity, fracture and yielding of cold compacted metal powders. Journal of the Mechanics and Physics of Solids 52, 1691–1717.

Martin, C.L., Bouvard, D., 2003. Study of the cold compaction of composite powders by the discrete element method. Acta Materialia 51, 373–386.

Martin, C.L., Bouvard, D., Shima, S., 2003. Study of particle rearrangement during powder compaction by the discrete element method. Journal of the Mechanics and Physics of Solids 51, 667–693.

Mesarovic, S.D., Fleck, N.A., 1999. Spherical indentation of elastic–plastic solids. Proceedings of the Royal Society of London A 455, 2707–2728.

Mesarovic, S.D., Fleck, N.A., 2000. Frictionless indentation of dissimilar elastic–plastic spheres. International Journal of Solids and Structures 37, 7071–7091.

Procopio, A.T., Zavaliangos, A., 2005. Simulation of multi-axial compaction of granular media from loose to high relative densities. Journal of the Mechanics and Physics of Solids 53, 1523–1551.

Skrinjar, O., Larsson, P.-L., 2004. On discrete element modelling of compaction of powders with size ratio. Computational Materials Science 31, 131–146.

Storåkers, B., Biwa, S., Larsson, P.-L., 1997. Similarity analysis of inelastic contact. International Journal of Solids and Structures 34, 3061–3083.

Storåkers, B., Fleck, N.A., McMeeking, R.M., 1999. The viscoplastic compaction of composite powders. Journal of the Mechanics and Physics of Solids 47, 785–815.

Vu-Quoc, L., Zhang, X., Lesburg, L., 2001. Normal and tangential force–displacement relations for frictional elasto-plastic contact of spheres. International Journal of Solids and Structures 38, 6455–6489.

Wu, C.-Y., Cocks, A.C.F., Gillia, O., 2003. Die filling and powder transfer. International Journal of Powder Metallurgy 39, 51–64.